



## Targeting HER2 + breast cancer cells: Lysosomal accumulation of anti-HER2 antibodies is influenced by antibody binding site and conjugation to polymeric nanoparticles

Shawn C. Owen<sup>a,c,d</sup>, Nish Patel<sup>b,e</sup>, Jennifer Logie<sup>a,c,d</sup>, Guohua Pan<sup>b,e</sup>, Helena Persson<sup>b,e</sup>, Jason Moffat<sup>b,e</sup>, Sachdev S. Sidhu<sup>b,e,\*</sup>, Molly S. Shoichet<sup>a,c,d,\*</sup>

<sup>a</sup> Department of Chemical Engineering & Applied Chemistry, University of Toronto, Toronto, Canada

<sup>b</sup> Banting and Best Department of Medical Research, University of Toronto, 160 College Street, Toronto, Ontario M5S3E1, Canada

<sup>c</sup> Institute of Biomaterials & Biomedical Engineering, University of Toronto, Toronto, Canada

<sup>d</sup> Department of Chemistry, University of Toronto, Toronto, Canada

<sup>e</sup> Donnelly Centre for Cellular and Biomolecular Research, University of Toronto, 160 College Street, Toronto, Ontario M5S3E1, Canada

### ARTICLE INFO

#### Article history:

Received 24 May 2013

Accepted 8 July 2013

Available online 21 July 2013

#### Keywords:

Antibody

Herceptin

Antibody–drug conjugate

Nanoparticle

### ABSTRACT

Humanized monoclonal antibodies (mAb) against HER2 are being engineered to treat cancer. We utilized phage-display technology to generate a novel anti-HER2 mAb (named 73JlgG) that binds an epitope of HER2 distinct from that of trastuzumab. Although these mAbs bind to the same cell surface receptor, they have different cell distribution profiles. After 3 h of incubation, almost 10% of the total 73JlgG reaches the lysosome compared to less than 3% of trastuzumab. Interestingly, 73JlgG disassociates from HER2 whereas trastuzumab remains bound to the receptor. Importantly, HER2 distribution is not affected by the antibody binding epitope, thus negating this mechanism as the reason for the difference in intracellular trafficking of 73JlgG versus trastuzumab. Each of trastuzumab and 73JlgG was chemically-modified with either a small molecule or polymeric nanoparticle to better understand the influence of conjugation on cellular localization. Relative to antibody alone, antibody–nanoparticle conjugates resulted in a higher concentration of antibodies in the lysosome whereas antibody–small molecule conjugates did not affect cell trafficking to the lysosome. Given the importance of lysosomal targeting, these results demonstrate the importance of understanding the influence of the antibody–conjugate on cell trafficking for ultimate optimization of treatment selection.

© 2013 Elsevier B.V. All rights reserved.

### 1. Introduction

The human epidermal growth factor receptor type 2 (HER2, also referred to as HER2/neu or ErbB2) is a member of the HER family of transmembrane receptor tyrosine kinases. Elevated levels of HER2 in cancer are associated with poor prognosis, and thus HER2 has become a major therapeutic target [1–3]. Trastuzumab (Herceptin®) is a humanized IgG used clinically to treat patients with HER2-dependent tumors [4]. Several mechanisms have been proposed to explain trastuzumab (Tras) activity and trafficking [5–7]. The conserved Fc region is important in recruiting immune cells, leading to antibody-dependent cell-mediated cytotoxicity (ADCC). Tras may prevent HER2 dimerization, or inhibit shedding of the extracellular domain (ECD) of HER2, both of which result in decreased signaling [8,9]. Tras may also decrease the cell surface levels of HER2 by increasing endosomal/

lysosomal destruction of the receptor [10]. Nevertheless, conflicting reports suggest that the majority of trastuzumab remains bound to HER2 and does not influence the internalization/recycling profile [11].

While the cell profile and mechanism of action of trastuzumab remain unclear, even less is known about newer anti-HER2 antibodies [5–7]. Several additional anti-HER2 antibodies are in development (i.e. pertuzumab and MM-111), each binding an epitope on HER2 that is unique from the Tras binding site [12–16]. We have used phage display technology to generate antibody libraries against a desired target [17,18] and herein describe the cellular disposition of one of these antibodies (73JlgG) that was generated against the ECD of HER2. Despite their proposed therapeutic mechanisms of action, the majority of therapeutic antibodies shows insufficient efficacy as a monotherapy and must be used concomitantly with additional chemotherapeutics. An exciting approach to increase the efficacy of therapeutic antibodies is to conjugate the antibodies with either potent, cytotoxic small molecule drugs [19–21] or with large drug-laden delivery vehicles (e.g. polymeric nanoparticles, liposomes, micelles) [22–28]. The first approach is designed to improve overall efficacy while maintaining desirable

\* Corresponding authors.

E-mail addresses: [sachdev.sidhu@utoronto.ca](mailto:sachdev.sidhu@utoronto.ca) (S.S. Sidhu), [molly.shoichet@utoronto.ca](mailto:molly.shoichet@utoronto.ca) (M.S. Shoichet).

pharmacokinetic (PK), therapeutic (e.g. ADCC, CDC), and targeting properties of the antibody [29]. The second approach is designed to utilize the antibody as a combined therapeutic and targeting ligand while delivering a high drug load preferentially to cancer cells [30].

Antibodies conjugated to small molecules (Ab–SM) bind to target antigens, facilitating endocytosis [31]. In fact, Tras has been derivatized with the cytotoxic agent maytansine (DM1) to produce the conjugate trastuzumab-DM1 (Tras-DM1), which is clinically approved for HER2-positive cancer [20,21]. The ability to internalize and traffic to the lysosome is important for Ab–SM conjugates to release the small molecule drug and for relevant cytotoxic pathways. For example, Tras-DM1 contains a non-reducible thioester bond between the antibody and drug, requiring internalization and proteolytic degradation of the conjugate in order for drug to be released [21,32]. Likewise, the Ab–SM brentuximab-vedotin (Adcetris®) has an enzymatically degradable linker between the parent antibody and drug, requiring this Ab–SM to reach the lysosome in order for the conjugated drug to be released and be efficacious [33,34].

Antibody–nanoparticle (Ab–NP) constructs are designed to bind specifically to the target cell via overexpressed antigens on the surface and then internalized through receptor-mediated endocytosis [30]. In this approach, the antibody is used as a therapeutic and targeting ligand; however, conjugation to nanoparticles may alter the pharmacokinetic profile and cell endocytosis mechanism of the parent antibody [35–37]. We studied cell endocytosis of Ab–NPs using polymeric nanoparticles comprised of self-assembled, amphiphilic poly(lactide-co-2-methyl, 2-carboxy-trimethylene carbonate)-graft-poly(ethylene glycol), P(LA-co-TMCC)-g-PEG. Previous studies with trastuzumab-modified P(LA-co-TMCC)-g-PEG NPs have shown specific binding and toxicity to HER2+ vs. HER2– cells [22,38].

To gain greater insight into antibody targeting and cellular distribution for Abs modified with either small molecules vs. nanoparticles, we compared a novel antibody (called 73JlgG and its corresponding fragment, 73JFab) to that of clinically approved trastuzumab (TraslgG, and its corresponding fragment, TrasFab) in terms of cell binding and lysosomal accumulation for the Ab alone, Ab–SM, and Ab–NP. While there has been a surge in popularity of antibody therapeutics and targeting ligands, there are few systematic studies that compare cellular distribution, even though cellular distribution impacts ultimate efficacy. Here we demonstrate that: 73JlgG (and 73JFab) bind an epitope on HER2 that is distinct from that of trastuzumab (and TrasFab); this binding is specific to HER2+ cells; and the cellular trafficking of 73JlgG differs from that of trastuzumab. We provide a quantitative analysis of the levels of trastuzumab and 73JlgG that remain bound to HER2, as well as the levels that reach the lysosome in two HER2+ cell lines. Interestingly, lysosomal accumulation is influenced by binding to nanoparticles. Developing a detailed understanding of cell trafficking for antibodies and emerging novel antibody drug or nanoparticle conjugates, will facilitate the selection of the most appropriate antibody system to achieve therapeutic efficacy.

## 2. Experimental

### 2.1. Materials

Herceptin® (trastuzumab) was purchased through Hoffmann-La Roche Limited (Mississauga, ON). The following antibodies were purchased: anti-LAMP2 [Rb] (Abcam 37024), anti-HER2 [Ms] (Thermo MS-301), anti-Rabbit 647 [Gt] (Invitrogen A2555A), anti-Mouse Alexa-546 [Gt] (Invitrogen A21043), and anti-Human IgG-H&L Fluorescein [Rb] (Sigma F4512). 5-((2-(and-3)-S-(acetylmercapto)succinoyl)amino) (SAMSA) fluorescein was purchased from Invitrogen (Eugene, OR). P(LA-co-TMCC)-g-PEG-furan was synthesized using previously reported protocols [39]. Sulfosuccinimidyl 4-(N-maleimidomethyl)cyclohexane-1-carboxylate (sulfo-SMCC) was purchased from Pierce (Rockford, IL).

All other solvents and reagents were purchased from Sigma-Aldrich and were used as received, unless otherwise noted.

### 2.2. Trastuzumab Fab

Trastuzumab Fab was produced from Trastuzumab IgG using a Fab Preparation Kit (Thermo Scientific Pierce, Rockford, IL) according to the manufacturer's guidelines.

### 2.3. Selection and characterization of anti-HER2 Fabs

Phage from Library F was cycled through rounds of binding selection with HER2 coated on 96-well Maxisorp Immunoplates (NUNC, Rochester, NY) as the capture target, as described [40]. After four rounds of selection, phage was produced from individual clones grown in a 96-well format and the culture supernatants were used in phage ELISAs to detect specific binding clones. Clones that bound to HER2 but not to bovine serum albumin (BSA; Sigma-Aldrich, St Louis, MO) were subjected to DNA sequence analysis.

### 2.4. Expression and purification of 73JFab protein

The Fab expression vector was derived from the phage display phagemid by inserting an amber stop codon upstream of the sequence encoding for cP3. Fab protein was produced by growing the transformed 55244 *Escherichia coli* cells as previously described [40]. The crude lysate was spun down, and the supernatant was applied to an rProtein affinity column (GE Healthcare); the column was washed with 100 column volumes of wash buffer (50 mM Tris-HCl, 150 mM NaCl, pH 8.0). Fab protein was eluted with nonpyrogenic elution buffer (50 mM NaH<sub>2</sub>PO<sub>4</sub>, 100 mM H<sub>3</sub>PO<sub>4</sub>, 140 mM NaCl, pH 2.8) and neutralized with nonpyrogenic neutralization buffer (1 M Tris-HCl, pH 8.0). Elutant was subsequently concentrated and buffer exchanged into PBS using the Amicon Ultra 30K Centrifugal Filters (Millipore, Carrigtwohill, CO) and protein concentrations were determined by a Nanodrop Spectrophotometer (Thermo Fisher Scientific, Wilmington, DE) using human Fab (Jackson ImmunoResearch, West Grove, PA) as a standard.

### 2.5. Conversion of 73JFab to 73JlgG1

The VH and VL sequences of the 73JFab clone were PCR-amplified and the resulting VL and VH cassettes were subcloned into EcoRI/BsiWI and EcoRI/NheI restriction sites in expression vector pFUSE2ss-CLlg-hk or pFUSEss-CHlg-hG1, respectively. Correct variable region sequences were verified by sequencing. Mammalian vector pFUSE2ss-CLlg-hk contains an expression cassette of the constant region of human  $\kappa$  light chain, and pFUSEss-CHlg-hG1 contains an expression cassette of the constant region of human  $\gamma$ 1 heavy chain (Invitrogen, San Diego, CA).

### 2.6. IgG production in mammalian cells

73JlgG1 was produced using the FreeStyle™ 293 Expression System as per manufacturer's instructions (Invitrogen, Burlington, ON, Canada). Briefly, 250 mL of 293F cells in suspension were cultivated in 1 L shaker flasks (Fisher Scientific, Ottawa, ON, Canada) to a density of  $\sim 1\text{--}1.2 \times 10^6$  cells/mL. For transfection, 250  $\mu$ g of the heavy chain DNA and 250  $\mu$ g of the light chain DNA were combined with 250  $\mu$ L of 293fectin and then added to the cells. Cells were fed  $\sim 24$  h after transfection with 0.5% (w/v) Tryptone (Bio Basic, Markham, ON, Canada) and harvested by centrifugation 5 days post-transfection. Conditioned medium was diluted with 1/10th volume of  $10\times$  PBS and incubated with 1 mL of rProtein A-Sepharose (GE Healthcare, Sweden) for 1 h at RT while shaking. The gravity-flow column was loaded with the conditioned media and the beads were washed with 100 CV of nonpyrogenic wash buffer ( $1\times$  PBS). IgG was eluted off the column with nonpyrogenic

elution buffer (0.2 M Arginine, pH 3.0) and neutralized with nonpyrogenic neutralization buffer (1 M Tris-HCl, pH 9.0). Elutant was subsequently concentrated and buffer exchanged into 1× PBS using the Amicon Ultra 30K Centrifugal Filters (Millipore, Carrigtwohill, CO). IgG was 0.2- $\mu$ m filtered and stored at 2–8 °C. Concentration and yield were determined by Nanodrop Spectrophotometer using human IgG (Jackson ImmunoResearch, West Grove, PA) as a standard.

## 2.7. Binding assays

96-well Maxisorp immunoplates coated with the ECDs of EGFR (HER1), HER2, HER3, and HER4 antigen (2  $\mu$ g/mL) were incubated with the purified Fab or IgG at a concentration of 200 nM. The wells were washed 8 times followed by incubation with horseradish peroxidase (HRP)-conjugated anti-kappa antibody for 30 min. The wells were washed 8 times followed by incubation with 3,3',5,5'-tetramethylbenzidine/H<sub>2</sub>O<sub>2</sub> peroxidase (TMB) substrate for 5–10 min. The reaction was stopped by adding 1 M H<sub>3</sub>PO<sub>4</sub> and the absorbance was measured spectrophotometrically at 450 nm in a microtiter plate reader. For epitope competition assays, 96-well Maxisorp immunoplates coated with the ECD of HER2 antigen (2  $\mu$ g/mL) were incubated with the purified Fab at a concentration of 200 nM for 1 h, and phage-Fab conjugates were added to the coated wells in the presence of the purified Fab for 20 min and assayed as described above using HRP-conjugated anti-M13 antibody.

## 2.8. IgG/Fab conjugation with SMCC

Anti-HER2 antibodies (2.5 nmol) were dialyzed for 24 h (20 kDa MWCO) against PBS buffer (10 mM, pH 7.4). Sulfo-SMCC (50 eq, 125 nmol) was added to the solution and left to react at room temperature for 4 h. The antibodies were dialyzed against PBS (10 mM, pH 7.4) for 24 h, changing the solution 4 times to remove unreacted sulfo-SMCC.

## 2.9. Antibody–small molecule (Ab–SM) preparation

SAMSA fluorescein (100  $\mu$ L, 10 mg/mL in DMSO) was activated by dissolving in NaOH (100  $\mu$ L, 0.1 M) and incubating for 15 min at room temperature. The SAMSA solution was neutralized with HCl (1.4  $\mu$ L, 6 M) and buffered with sodium phosphate (20  $\mu$ L, 500 mM, pH 7). Antibody–SMCC conjugates were reacted with activated SAMSA fluorescein (10 eq) for 30 min at room temperature followed by purification by dialysis for 24 h (20 kDa MWCO) against PBS buffer (10 mM, pH 7.4). Antibody–SM were further purified by size exclusion chromatography on a Sephadex G-25 column (GE Healthcare, United Kingdom). The degree of labeling was calculated by quantifying SAMSA using absorbance at 494 nm with an extinction coefficient of 80,000 M<sup>-1</sup>·cm<sup>-1</sup>.

## 2.10. Antibody–nanoparticle (Ab–NP) preparation

P(LA-co-TMCC)-g-PEG-furan micelles were prepared as previously reported [39,41]. To prepare immune–micelle conjugates, pre-formed micelles (2 mg/mL, 50 nmol) were reacted for 24 h with IgG/Fab SMCC (2 mg/mL, 100 nmol) in MES buffer (100 mM, pH 5.5, 100  $\mu$ L). Free Ab was purified from Ab–NP by Fast Protein Liquid Chromatography (FPLC) performed on an ÄKTApurifier system (GE Healthcare, United Kingdom) equipped with a Superdex 200 column. The column was equilibrated with distilled water for 20 min and PBS buffer (10 mM, pH 7.4) for 20 min at a flow rate of 1.5 mL/min before use. Isocratic elution was carried out in PBS buffer (10 mM, pH 7.4) and fractions containing the micelles and/or free IgG/Fab were detected by absorbance at 260 nm and 280 nm respectively. Quantification of antibody substitution levels was performed as previously described [42]. Briefly, the concentration of NP polymer is held constant for all samples and the antibody in each Ab–NP is calculated based on

absorbance at 280 nm (for IgG  $\epsilon_{280}$  = 210,000 M<sup>-1</sup>·cm<sup>-1</sup>, for Fab  $\epsilon_{280}$  = 83,800 M<sup>-1</sup>·cm<sup>-1</sup>) [43], correcting for any contribution from the NP at the same wavelength. The number of antibodies per NP is based on an aggregation number of 3500 polymer chains/NP [42].

## 2.11. Zeta potential

Zeta potential was measured by a Malvern Zetasizer Nano ZS, equipped with a 4 mW, 633 nm laser. Samples were measured using folded capillary cells (Malvern, DTS 1060). The average and standard deviation are reported for 3 individual samples, prepared under the same conditions with 36 runs each. All samples have a concentration of ~1 mg/mL and were filtered through a NY-0.45  $\mu$ m filter (Progene, QC, Canada) prior to measurement.

## 2.12. Cell culture

293F cells (Gibco, Burlington, ON, Canada) were maintained in Gibco® CD 293 medium. SKBR-3 cell line (purchased from ATCC) was maintained (<8 passages) in a tissue culture incubator (37 °C, 5% CO<sub>2</sub>, 95% humidified) in plastic culture flasks in McCoy's 5A growth medium supplemented with 10% FBS, 10 UI/mL penicillin, and 10  $\mu$ g/mL streptomycin. HER2+ cell line BT-474, and HER2– cell lines MDA-MB-231, MCF-7, and T47D were maintained (<8 passages) in RPMI 1640 growth medium supplemented with 10% FBS, 10 UI/mL penicillin, and 10  $\mu$ g/mL streptomycin. Cells were seeded at 10,000 cells/cm<sup>2</sup> in 8-chamber Lab-Tek® culture slides (Rochester, NY) and allowed to adhere overnight. Cells were treated with free antibody, Ab–SM, or Ab–NP formulations in media for 3 h. All antibodies, Ab–SM and Ab–NPs were used at 50 nM based on the antibody concentration as determined by absorbance measurements at 280 nm. Geldanamycin was used at 2  $\mu$ M from a stock solution of 2 mM in DMSO.

## 2.13. Immunofluorescence

After treatment, cells were washed twice with fresh media for 10 min, twice with PBS for 5 min, and then fixed in 4% paraformaldehyde (PFA) for 1 h at room temperature. Fixed cells were washed three times with PBS for 5 min and then incubated with PBS containing 0.5% saponin for 10 min. Cells were again washed and then incubated with 1% BSA in PBS containing 0.05% Tween 20 (PBST) for 30 min. Samples were then incubated sequentially with diluted primary antibodies – anti-LAMP2 [Rb] (Abcam 37024); and anti-HER2 [Ms] (Thermo MS-301) in 1% BSA in PBST for 1 h at room temperature. Cells were incubated sequentially with secondary antibodies – anti-Rabbit 647 [Gt] (Invitrogen A2555A); anti-Mouse Alexa-546 [Gt] (Invitrogen A21043); and anti-Human Fab H&L Fluorescein [Rb] (Sigma F4512) in 1% BSA in PBST for 1 h at room temperature. Cells were washed several times with 1% BSA in PBST and PBS between antibody incubations. Samples were mounted in media containing DAPI (Vectasheild®, Vector Laboratories, Burlingame, CA).

## 2.14. Flow cytometry

After treatment, cells were washed twice with fresh media for 10 min and twice with 1× PBS for 5 min. Cells were incubated with 0.05% trypsin, 5.3 mM EDTA in PBS for 5 min at 37 °C and then detached with a rubber spatula. Cells were sedimented at 800× g and then washed 4 times in PBST with sedimenting between washings. Samples were treated with 1% BSA in PBST for 5 min and again washed 4 times in PBST. Cells were then incubated with anti-human IgG-H&L Fluorescein [Rb] (Sigma F4512) or anti-human kappa light chain Alexa-555 for 30 min in the dark. Cells were again washed several times as previously, resuspended in Hanks Balanced Saline Solution (pH 7.4) and treated with 7-aminoactinomycin D (7AAD) (1:1000 dilution). Data was

acquired on Flow Cytometry (Canto, Becton-Dickinson) and analyzed with FlowJo software (Tree Star, Inc., Ashland, OR).

### 2.15. Surface plasmon resonance

The kinetic parameters and dissociation constants for interactions between Fabs and recombinant HER2 ECD fused to Fc (HER2–Fc) (R&D Systems) were measured by SPR using a ProteOn XPR36 instrument (Bio-Rad). HER2–Fc was immobilized on a GLC chip by standard amine coupling chemistry and serial dilutions of Fab or IgG in PBS at pH 7.4 or pH 6.0 with 0.05% Tween 20 were injected over the HER2–Fc and blank channels (for reference subtraction) for 60 s at a flow rate of 100  $\mu\text{L}/\text{min}$ , followed by 10 min of buffer to monitor Fab dissociation. The chip surface was regenerated with 0.85%  $\text{H}_3\text{PO}_4$  prior to new analyte injection. Kinetic parameters were determined by globally fitting a reference cell-subtracted concentration series to a 1:1 (Langmuir) binding model.

### 2.16. Confocal imaging and processing

Images were collected by confocal microscopy on an Olympus FV1000 at 60 $\times$  magnification, using the following excitation and emission wavelengths: for DAPI, excitation at 405 nm, emission at 460 nm; for Alexa-488 and fluorescein, excitation at 485 nm, emission at 520 nm; for Alexa-546, excitation at 560 nm, emission at 580 nm; and for Alexa-647, excitation at 650 nm, emission at 675 nm. Z-stacks of cells were collected with 0.5  $\mu\text{m}$  steps between images and all planes from the z-stacks were quantified. Colocalization studies were performed using Olympus FV1000-ASW software by computing the overlap of individual pixels from two fluorescence channels. Thresholds were set from negative control experiments using cells treated with secondary antibodies only to account for non-specific fluorescence. The software provides a scattergram display of each pixel in the image, which can be gated to determine and quantify colocalized pixels (Fig. 1) [44]. The colocalization is also depicted as a separate “channel” overlay to provide qualitative information of the cell structures where both molecules are located (Fig. 1E).

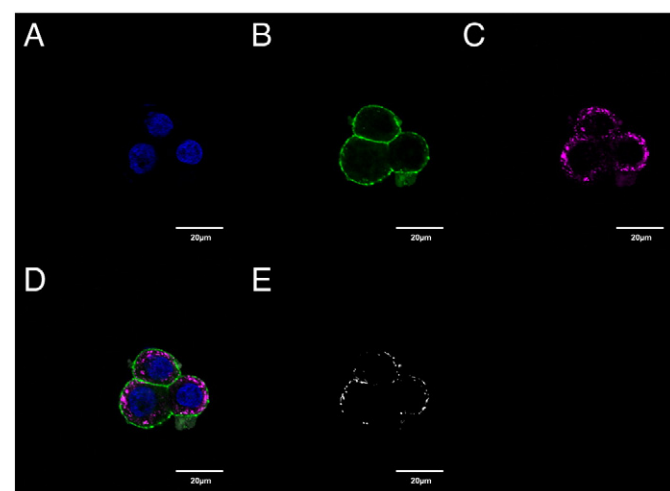


**Fig. 1.** Representative confocal image (single specimen plane) of HER2 positive cells (SKBr-3). A) Cell nuclei (blue, DAPI); B) anti-HER2 antibody trastuzumab is shown mainly localized at the cell surface (green, anti-Human IgG); C) lysosomes (magenta, anti-LAMP2); D) composite overlay of nuclei, antibody, and lysosomes; and E) overlapping regions (shown as white) depicting the overlapping regions of the antibodies (green) and lysosomes (magenta). In this image, 3.5% of the total Tras is found to colocalize with lysosomes as calculated from scatterplots of individual image pixels (scale bar = 20  $\mu\text{m}$ ).

### 2.17. Graphing and statistics

All statistical analyses were performed using GraphPad Prism version 5.00 for Windows (GraphPad Software, San Diego California USA, [www.graphpad.com](http://www.graphpad.com)). Differences among groups were assessed by one-way ANOVA with Bonferroni *post hoc* correction to identify statistical differences among three or more treatments. Alpha levels were set at 0.05 and a p-value of  $\leq 0.05$  was set as the criteria for statistical significance. Graphs are annotated where p-values are represented as \* $p \leq 0.05$ , \*\* $p \leq 0.01$ , or \*\*\* $p \leq 0.001$ . All data are presented as mean  $\pm$  standard deviation.

## 3. Results

### 3.1. Synthetic antibody generated from phage display library binds specifically to HER2

We constructed a highly optimized antibody library by structure-based design using phage-display technology. Individual clones from a pool of specific binders were used in phage ELISAs to identify specific binding clones to recombinant HER2. Clones that bound specifically to HER2 were subjected to DNA sequence analysis and the phage display phagemids were converted into expression vectors for Fab protein purification. The selection produced antibodies with tight affinities in the low-nanomolar range against HER2. One of these novel anti-HER2 antibodies was selected for further study, hereafter referred to as “73J”. We synthesized both the antibody binding fragment (73JFab) and the whole antibody in the human IgG1 format (73JIgG). The complementarity determining region (CDR) sequences of 73J are shown in comparison to those of trastuzumab in Fig. 2 (variable regions (Fv) sequences are shown in Supplemental Fig. S1).

We first examined the specificity of 73J binding to HER2 *in vitro*, while also confirming the specificity of TrasIgG and TrasFab, by measuring the binding to ECDs of each of the four HER family members. Both the 73JFab and 73JIgG bind specifically to the ECD of HER2 but not we tested whether 73J binds to a HER2 epitope that is different from that of trastuzumab. Pre-treatment with 73JFab prevented the subsequent binding of 73J-phage but did not block trastuzumab-phage (Trasphage) binding (Fig. 3B). Similarly, pre-treatment with trastuzumab Fab (TrasFab) prevented the binding of Tras-phage but not 73J-phage.

We further verified the specificity of 73JIgG for HER2 on cell surfaces using flow cytometry. Consistent with ECD binding studies, we observed a shift in the fluorescence population for all antibodies in the HER2 + cell line, SKBr-3 (Supplemental Fig. S2) [45]. A similar shift in fluorescence staining was not observed in the HER2-negative cell line, MDA-MB-231. We analyzed the binding of IgG/Fabs to SKBr-3 cells to determine if the difference in cell trafficking is related to the level or degree of binding. Quantification of flow cytometry spectra confirms that there is no difference in the number of cells that bind TrasIgG and 73JIgG or TrasFab and 73JFab (Fig. 3C). We found that in all cases, 85% of the live cell populations are positive for ligand binding and that there are no differences between each of the binding levels of TrasIgG and 73JIgG and between TrasFab and 73JFab forms; however, there is a significant difference between each IgG and its respective Fab ( $p < 0.001$  for Tras and  $p < 0.05$  for 73J). Importantly, there is no significant difference in antibody binding levels after incubating with SKBr-3 cells for either 3 h or 12 h (Fig. 3C), and thus all subsequent studies were conducted at 3 h.

We confirmed the specificity of 73J for HER2 presented on cell surfaces by immunofluorescent staining (IF). Fluorescent staining of 73JIgG and Tras was observed for the HER2-positive breast cancer cell lines, SKBr-3 and BT-474, but not the HER2-negative cell lines, T47D and MCF-7 (Supplemental Fig. S3). Collectively, these results demonstrate that the anti-HER2 antibody, 73JIgG, like Tras, binds specifically to HER2 presented on cell surfaces.

Fab	CDRL1				CDRL2				CDRL3									
	28	29	30	32	50	51	52	54	55	91	92	93	94	95	96	97		
Trastuzumab	D	V	N	T	A	S	A	S	F	L	Y	H	Y	T	P	P	T	
73J	S	V	S	S	A	S	A	S	S	L	L	G	Y	Y	P	P	F	T

Fab	CDRH1				CDRH2				CDRH3																					
	28	29	30	31	32	33	34	35	50	51	52	52a	53	54	55	56	57	58	95	96	97	98	99	100	100a	100b	100c	101	102	
Trastuzumab	N	I	K	D	T	Y	I	H	R	I	Y	P	T	N	G	Y	T	R	W	G	G	D	G	F	Y	A	M	D	Y	
73J	N	L	Y	S	S	Y	I	H	S	I	Y	P	Y	S	S	Y	T	S	Y	Y	G	F	A	M					D	Y

**Fig. 2.** The amino acid sequences of the complementary determining regions (CDR) of the heavy (H) and the light (L) chain of 73JlgG and trastuzumab.

Kinetic analysis of the purified Fabs and IgGs by Surface Plasmon Resonance (SPR) showed that the antibodies bind to recombinant HER2 with high affinities (Table 1) with  $K_D$  values ranging from 0.50 nM to 3.25 nM at neutral pH. Moreover, we show that the binding kinetics of the purified antibodies is not significantly altered at a lower pH of 6.0 which has been reported as the pH for the early endosome [46].

### 3.2. Trafficking studies reveal a difference in anti-HER2 ligand distribution

Confocal image analysis for HER2-positive (SKBr-3) cell lines qualitatively shows that the majority of antibodies are found on the cell

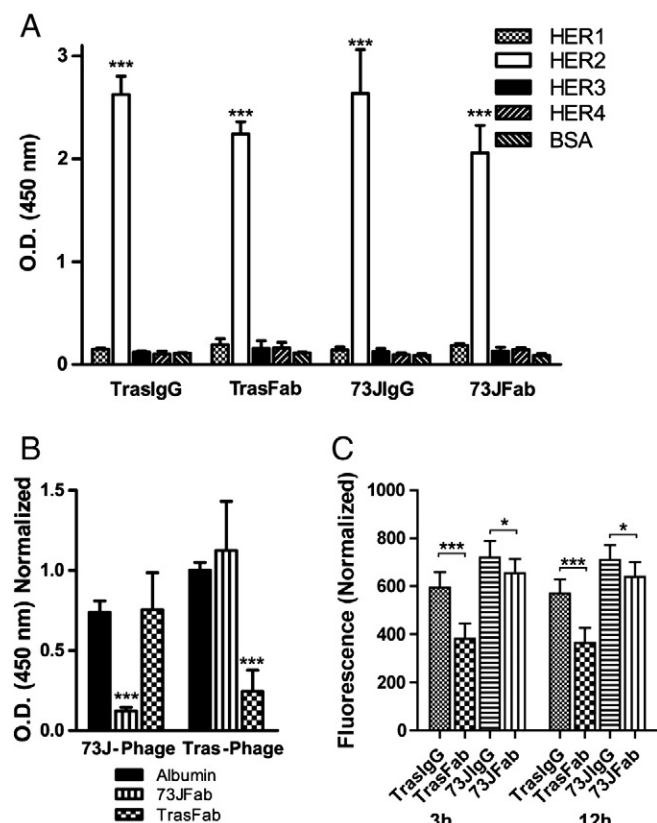


**Fig. 3.** Binding properties of trastuzumab and 73J. A) IgG and Fab forms of 73J and trastuzumab bind to HER2 but not to other members of the HER family (mean  $\pm$  SD,  $N = 3$ , \*\*\* $p < 0.001$ ). B) Trastuzumab and 73J bind to different epitopes on HER2. Immobilized ECD of HER2 was first incubated with one of TrasFab or 73JFab (10  $\mu$ g/mL) or BSA as control and then treated with phage-displayed 73JFab or TrasFab (phage-73J or phage-Tras). Plates were assayed for immobilized Fab-phage complexes using HRP-conjugated anti-phage antibody. Pre-treatment with each antibody blocks binding of its cognate Fab-phage but not the other Fab-phage (mean  $\pm$  SD,  $N = 4$ , \*\*\* $p < 0.001$ ). C) Quantification of antibody binding to HER2 positive cells (SKBr-3) by flow cytometry, with fluorescence normalized to number of fluorophores per antibody. There is no significant difference in binding levels between 73J and trastuzumab (Tras) in either IgG or Fab forms; however, there are significant differences between IgG and Fab forms of both trastuzumab and 73JlgG. In addition, there is no difference in antibody binding after 3 h or 12 h of incubation (mean  $\pm$  SD,  $N = 6$ , \*\*\* $p < 0.001$ , \* $p < 0.05$ ).

surface (Fig. 4A). To elucidate differences in cell distribution of the anti-HER2 ligands, we quantified the levels of IgG/Fab that reach the lysosome after 3 h using colocalization studies. We selected 3 h as a representative time point because: 1) we measured no difference in binding levels between 3 h and 12 h of incubation (Fig. 3C); 2) previous studies have shown that trastuzumab cell distribution reaches steady state between 2 and 4 h and that the maximum level of internalization is detected at 3 h [7]; and 3) previous studies have shown that anti-HER2 conjugation to nanoparticles does not affect their binding to HER2+ cells [38]. We used a secondary antibody (anti-human Fab H&L) to visualize the location of anti-HER2 Fabs and IgGs and an anti-lysosomal membrane (LAMP2) antibody to visualize the location of lysosomes. The percent of total 73JlgG that localizes to the lysosome ( $9.5 \pm 1.2\%$ ) is significantly greater ( $p < 0.05$ ) than any other antibody ligand form tested for both cell types tested: 73JFab, TrasFab and TrasIgG all localized to the lysosome at less than 3.0% for SKBr-3 cells and less than 5.0% for BT-474 cells (Fig. 4B).

Further evidence that the anti-HER2 ligands are on the surface and in recycling endosomes is seen from blocking experiments using the heat-shock protein inhibitor, geldanamycin (Supplemental Fig. S4A). Geldanamycin does not stimulate or alter the rate of HER2 endocytosis, but instead blocks HER2 recycling and changes endosomal sorting, forcing more HER2 to be trafficked to lysosomes [7,47]. In the presence of geldanamycin, the amount of ligand at the cell surface decreases and the amount of ligand in the lysosome increases significantly in all cases compared to untreated cells ( $p < 0.001$ ). In addition, there is no difference between the amounts of each ligand found in lysosomes after geldanamycin treatment (Supplemental Fig. S4B).

### 3.3. HER2 distribution is not affected by antibody binding, yet 73JlgG disassociates from HER2

We explored whether the difference in cell distribution observed for 73JlgG was linked to a change in the trafficking of HER2. One debated mechanism of action for trastuzumab is the downregulation of surface HER2; specifically, the binding of trastuzumab may induce HER2 internalization and sorting to the lysosomal pathway instead of recycling. Considering that our novel anti-HER2 73JlgG binds to unique epitopes on HER2, this unique binding may impact the rate of HER2 downregulation. Therefore, we quantified the amount of HER2 in the lysosome.

We performed colocalization experiments of HER2 and lysosome by first treating cells with one of TrasIgG, TrasFab, 73JlgG or 73JFab for 3 h and then fixing the cells. Fixed cells were fluorescently labeled to track the location of HER2 (using anti-HER2 antibody with a distinct binding site from Tras and 73JlgG) and lysosomes (using anti-LAMP2 antibody). In all treatments, as well as untreated controls, we found that less than 10% of HER2 is localized with the lysosomes (Fig. 5A), suggesting that HER2 trafficking is not affected by binding to Tras or 73J antibodies ( $p = 0.71$  between formulations).

We determined the difference in cell distribution of antibodies by quantifying the amount of antibody that colocalizes with HER2. Our results show that the amount of 73JlgG that remains bound to HER2 is

**Table 1**

Binding affinities of antibodies to HER2 under different pH determined by Surface Plasmon Resonance (SPR).

Antibody	pH	$k_{on}, s^{-1} \cdot M^{-1}$	$k_{off}, s^{-1}$	$K_D, nM$
TrasIgG	6.0	$4 \times 10^5$	$2 \times 10^{-4}$	$0.50 \pm 0.01$
	7.4	$2 \times 10^5$	$1 \times 10^{-4}$	$0.50 \pm 0.01$
TrasFab	6.0	$2 \times 10^5$	$1 \times 10^{-4}$	$0.44 \pm 0.01$
	7.4	$9 \times 10^4$	$9 \times 10^{-5}$	$1.06 \pm 0.05$
73JlgG	6.0	$7 \times 10^5$	$8 \times 10^{-4}$	$1.18 \pm 0.03$
	7.4	$5 \times 10^5$	$7 \times 10^{-4}$	$1.37 \pm 0.02$
73JFab	6.0	$6 \times 10^5$	$1 \times 10^{-3}$	$2.24 \pm 0.05$
	7.4	$4 \times 10^5$	$1 \times 10^{-3}$	$3.26 \pm 0.06$

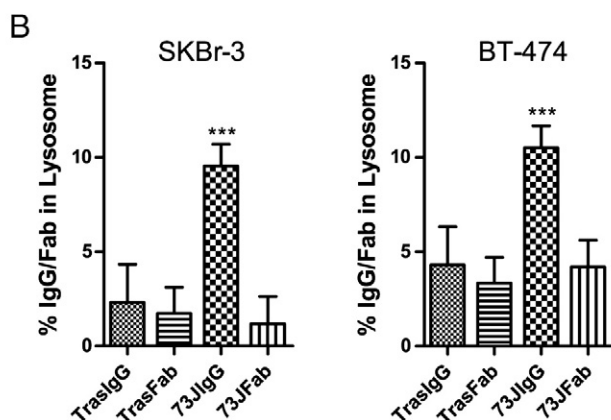
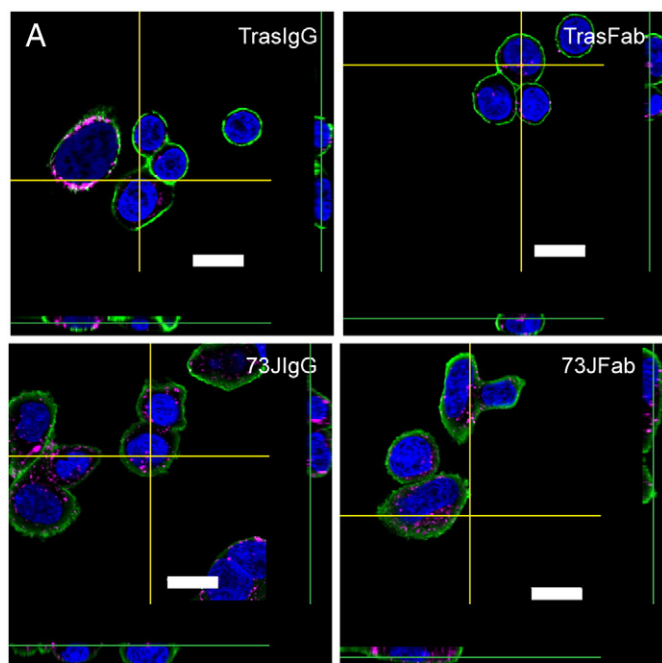


**Fig. 4.** Cell trafficking of Fab and IgG forms of anti-HER2 antibodies. A) Representative confocal image cross-sections of HER2 positive cells (SKBr-3) show the anti-HER2 antibodies mainly localized at the cell surface (green, anti-Human IgG), while lysosomes (magenta, anti-LAMP2) and cell nuclei (blue, DAPI) are internal (scale bar = 20  $\mu$ m, bottom and right of each figure show the side view of z-stacked images corresponding to the yellow cross hairs); B) the amount of antibody that colocalizes with lysosomes was quantified from fluorescence confocal images (see *Experimental* section for details). Nearly 10% of the total 73JlgG is found within lysosomes, compared to less than 3% of other IgG/Fabs for SKBr-3 cells and less than 5% of other IgG/Fabs for BT-474 cells (mean  $\pm$  SD, N = 4, \*\*\*  $p < 0.001$ , 3 h incubation).

significantly lower than other ligands ( $p < 0.001$ ). Only  $52.77 \pm 11.01\%$  of 73JlgG remains associated with HER2 after 3 h of treatment compared to  $84.77 \pm 9.35\%$  for TrasIgG,  $92.43 \pm 2.57\%$  for TrasFab, and  $85.59 \pm 3.45\%$  for 73JFab (Fig. 5B). This result confirms that 73JlgG dissociates from HER2 and suggests that 73JlgG is trafficked to the lysosome in an unbound form.

#### 3.4. Preparation of antibody–small molecule (Ab–SM) and antibody–nanoparticle (Ab–NP) conjugates

The IgG and Fab forms of each antibody were first modified with SMCC thereby providing a functional maleimide for conjugation to either small molecules or nanoparticles through thiol–maleimide click chemistry (Fig. 6). This chemistry is similar to that of the clinically approved antibody–drug conjugate T-DM1, where SMCC-modified trastuzumab is coupled with thiolated maytansine [19,48], and is thus

highly relevant. For this study, we conjugated two maleimides per antibody, similar to other antibody–drug conjugates [21].

To prepare Ab–NP conjugates, we used the same maleimide-functionalization of the antibodies followed by a Diels–Alder click reaction with furan-modified polymeric nanoparticles prepared from P(LA-co-TMCC)-g-PEG-furan as previously described (Fig. 6B) [38]. Ab–NPs were purified from unconjugated antibody using size exclusion FPLC and analyzed to determine changes in size and degree of conjugation. On average,  $\sim 200$  antibodies were conjugated per nanoparticle and there was no significant change in the measured size of nanoparticles before ( $100 \pm 10$  nm) and after ( $105 \pm 12$  nm) conjugation, as determined by dynamic light scattering (DLS). The zeta potential of the nanoparticles also remained unchanged at  $-21.1$  mV  $\pm 1.40$  mV (mean  $\pm$  standard deviation,  $n = 3$ ).

#### 3.5. Small molecule conjugation to antibodies does not affect lysosomal accumulation

We compared the levels of antibody accumulation in the lysosome to Ab–SM levels and found that conjugation of a small molecule to the parent antibody does not significantly alter lysosomal accumulation (Fig. 7). Although there is a modest trend of increasing lysosomal concentration of antibody after small molecule conjugation, the difference between Ab–SM and the parent antibody is not statistically significant in either of the cell lines tested: SKBr-3 and BT-474 (Fig. 7B, C). For TrasIgG–SM, TrasFab–SM and 73JFab–SM, approximately 5% of the total antibody concentration is found in the lysosome. Consistent with the results for parent antibody distribution, the amount of 73JlgG found in the lysosome is greater than all other forms, at approximately 10%; however, there is no significant difference between unmodified 73JlgG and 73JlgG–SM forms.

#### 3.6. Conjugation of antibodies to nanoparticles results in greater accumulation in lysosomes

We explored whether the conjugation of antibodies to  $\sim 100$  nm polymeric nanoparticles altered the intracellular trafficking of the unmodified antibody. Following the same methods described for Ab–SMs, HER2-positive cell lines were incubated with Ab–NP conjugates and the levels of lysosomal accumulation were quantified after 3 h using confocal microscopy (Fig. 8A). In distinct contrast to Ab–SM modification, the amount of Ab–NP that is trafficked to the lysosome is significantly greater than the parent antibody for all forms

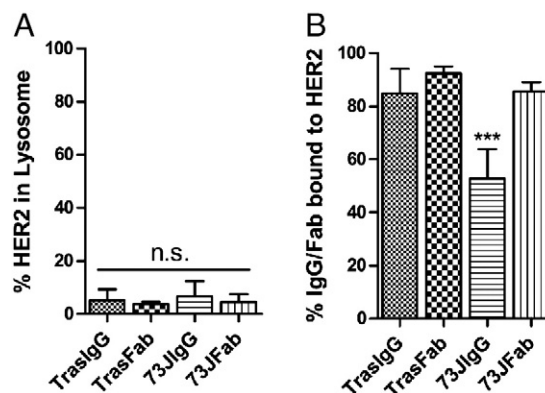


**Fig. 5.** Trastuzumab or 73J binding does not induce lysosomal accumulation of HER2. A) The amount of HER2 that colocalizes with lysosomes upon treatment with the indicated antibodies is the same and independent of the antibody tested (mean  $\pm$  SD, N = 6,  $p = 0.71$ ). B) Colocalization of antibodies with HER2 after 3 h of treatment: 80–90% of each of TrasIgG, TrasFab and 73JFab remains bound to HER2 whereas only  $\sim 50\%$  of the 73JlgG colocalizes with HER2, suggesting that 73JlgG dissociates from HER2 in the endosome and traffics to the lysosome as unbound ligand. The amount of antibody that colocalizes with lysosomes was quantified from fluorescence confocal images (mean  $\pm$  SD, N = 6, \*\*\*  $p < 0.001$ ).

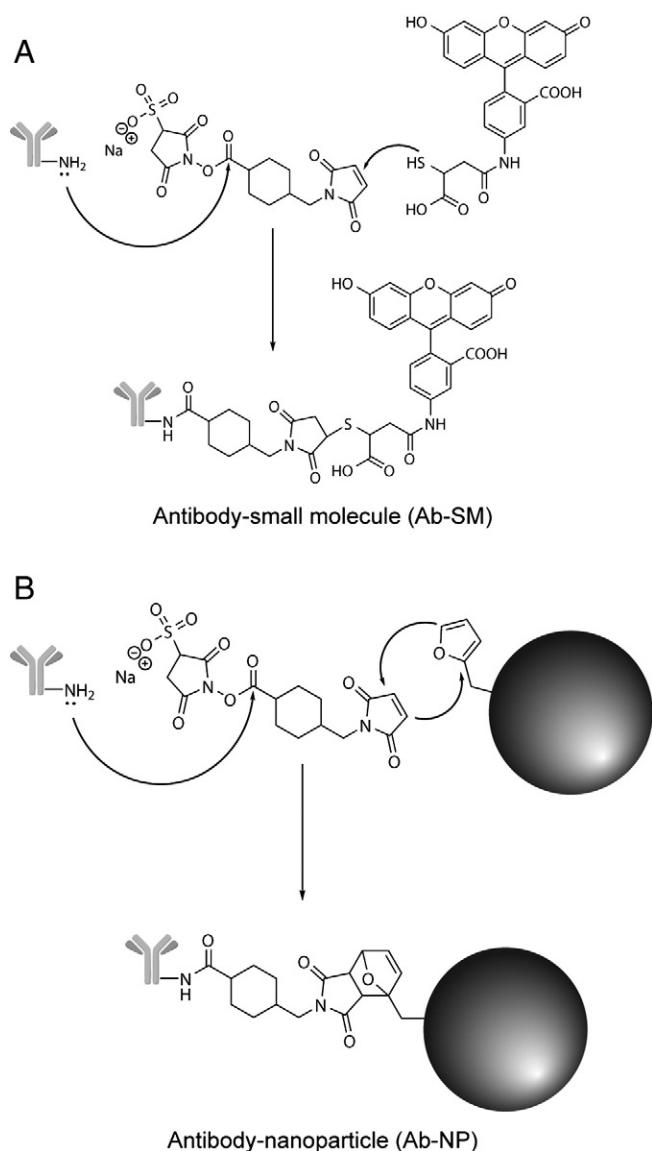


**Fig. 6.** Antibody-conjugates were prepared through click chemistry reactions. A) Antibody–small molecules (Ab-SM) were prepared from a thiol-containing fluorophore using thiol–maleimide chemistry. IgG was first reacted with SMCC to provide a functional maleimide and then reacted with SAMS–fluorescein. B) Antibody–nanoparticle (Ab-NP) conjugates were synthesized from IgG/Fab–maleimide, which was synthesized by reaction of IgG/Fab with SMCC, and (LA-co-TMCC)-g-PEG–furan nanoparticles using Diels–Alder click chemistry.

( $p < 0.001$ ). For TrasIgG, TrasFab, and 73JFab, the amount of lysosomal accumulation increases from approximately 5% for unmodified antibody to approximately 10% for Ab-NP in both of the cell lines tested (Fig. 8B, C). Similarly, for 73JIgG, the amount of lysosomal accumulation increases from approximately 10% for unmodified antibody to approximately 15% for Ab-NP for both of the cell lines tested. Thus, the percent of 73JIgG that localizes to the lysosome is significantly greater than all other forms, in both cell types and regardless of the conjugated cargo. Previous studies have demonstrated that anti-HER2 Ab-NP specifically binds to HER2+ cells and that binding is required for internalization [38].

#### 4. Discussion

We produced a novel anti-HER2 antibody, 73J using phage-display screenings. From ELISA and cell-based studies we show that 73JIgG

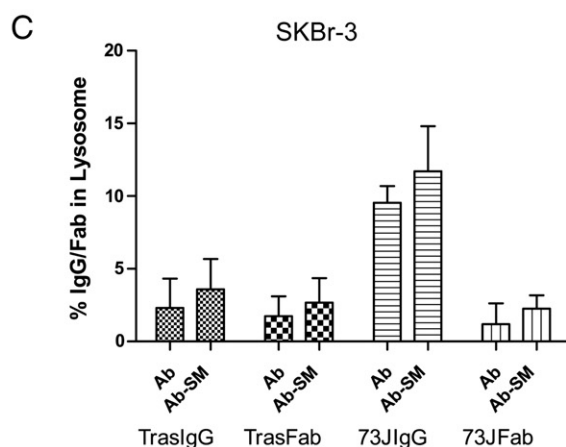
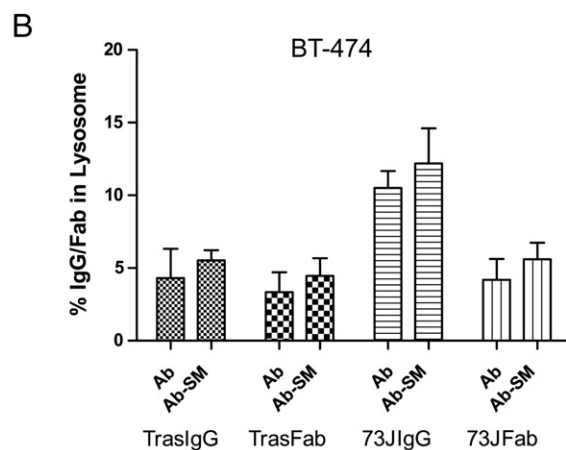
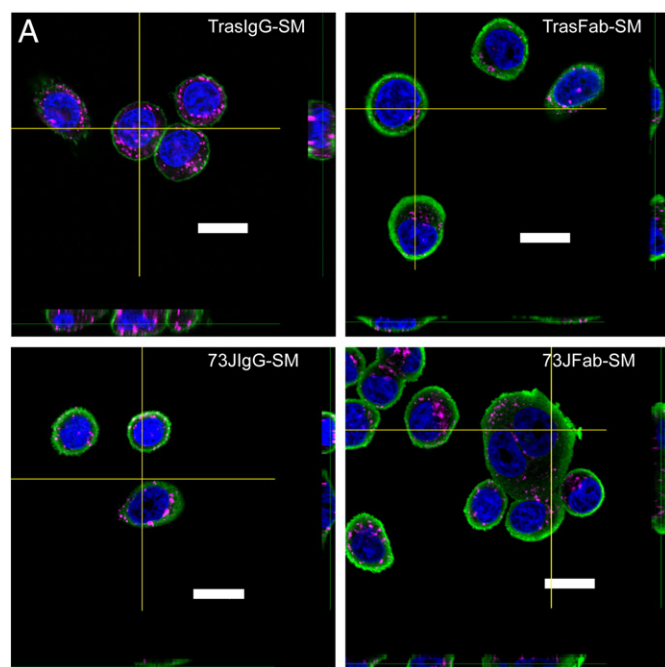


**Fig. 7.** Ab-SM conjugates traffic to lysosomes at similar levels to the parent antibody. A) Representative confocal images of HER2 positive BT-474 cells show the location of anti-HER2 antibodies (green, anti-Human Fab), lysosomes (magenta, anti-LAMP2) and cell nuclei (blue, DAPI) (scale bar = 20  $\mu$ m). Distinct, punctate bodies seen in the images are indicative of lysosomal compartments. B, C). Conjugation with a small molecule (Ab-SM) does not significantly alter the amount of antibody that co-localizes with lysosomes in BT-474 or SKBr-3 cell lines (mean  $\pm$  SD,  $N = 6$ ,  $p = 0.50$ ); however there are significant differences between TrasIgG-SM and 73JIgG-SM as there are between the parent antibodies.

and 73JFab bind to the ECD of HER2 with equal specificity and efficiency as trastuzumab. The 73J antibody binds to a different epitope on HER2 than that of trastuzumab and, although these two antibodies bind the same cell surface receptor, their accumulation in the lysosome is different as is the way they are trafficked. Thus, we demonstrate, for the first time, that the HER2 epitope binding site has an impact on downstream trafficking, which suggests that HER2 antibody-based therapy can be tailored for a desired mechanism of action or subcellular target [49]. Specifically, the enhanced lysosomal targeting of IgG relative to trastuzumab and other anti-HER2 antibodies may allow drugs bound there to be more effectively delivered to an intracellular organelle or protein [19].

The difference in lysosomal accumulation of the two antibodies is not a result of limited HER2/antibody complex internalization. Treatment with geldanamycin impairs endosomal recycling causing the amount of HER2/antibody complex on the cell surface to dramatically decrease, and the amount internalized to increase. By blocking endosomal recycling, the internalized HER2/ligand should be forced into the lysosomal pathway and, indeed, there are significantly more antibodies in lysosomes after blocking, with more than 15% of each antibody in the lysosome. Binding to either epitope does not exclude HER2 from the normal internalization mechanisms.

One currently proposed mechanism of action of trastuzumab is the down-regulation or decrease of cell-surface HER2 levels. Thus, we hypothesized that antibody binding to HER2 would alter the cellular distribution of the receptor. Similar to geldanamycin treatment, an induced decrease in cell-surface levels of HER2 from antibody binding should correspond to an increase in lysosome levels of HER2. However, we observed no significant change in the location of HER2 after antibody binding – the amount of HER2 found in the lysosome did not increase after ligand binding. This result suggests that antibody binding itself has no impact on the distribution of HER2 over the duration of the experiment, but rather where the antibody binds is more important. Binding a distinct epitope from trastuzumab may also provide concomitant or secondary therapy to overcome trastuzumab resistance that has been proposed to arise from epitope masking [50].

Intriguingly, we found that the amount of 73JlgG that colocalizes with HER2 is significantly lower than the other ligands tested, and since we observe more 73JlgG in the lysosome, it is likely that 73JlgG disassociates from HER2 in the endosome and is then alone trafficked to the lysosome. We did not observe a significant difference in binding affinity between IgG and HER2 as a function of pH, and thus the disassociation is unlikely to be related to the characteristic drop in pH of the endosome. Other environmental changes in the endosome, such as salt concentration, may have an impact on the binding affinity. Although the exact mechanism by which 73JlgG disassociates is unclear, this new anti-HER2 antibody shows higher lysosomal accumulation than trastuzumab and thus promises to increase the delivery of conjugated payloads.

We investigated the effects of conjugation of two anti-HER2 antibodies (trastuzumab vs. 73JlgG) to either a small molecule or a polymeric nanoparticle on intracellular trafficking. We used a small molecule containing a free thiol (SAMSA) to mimic the linkage chemistry employed in the antibody–drug conjugate, T-DM1 [19]. For Ab-NP conjugates, we used orthogonal Diels–Alder “click” chemistry to couple maleimide-activated antibodies with furan-activated nanoparticles. The conjugations used to couple the antibodies to small molecules and nanoparticles were performed under mild aqueous conditions, thereby preserving the native structure of both the antibodies and pre-assembled polymeric nanoparticles. In agreement with previous studies, the conjugation of anti-HER2 antibodies to NP is requisite and specific for uptake by HER2+ cells.

Many antibody–drug conjugates are designed to impart two distinct therapeutic mechanisms on target cells – one from the antibody itself (e.g. ADCC, CDC) and one from the conjugated drug. Importantly, we demonstrate that appending a small molecule to these antibodies

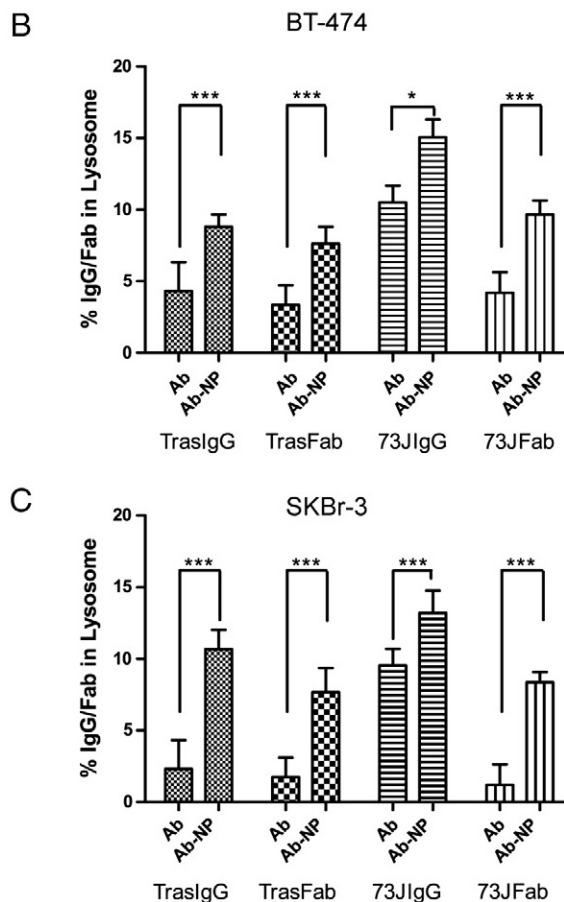
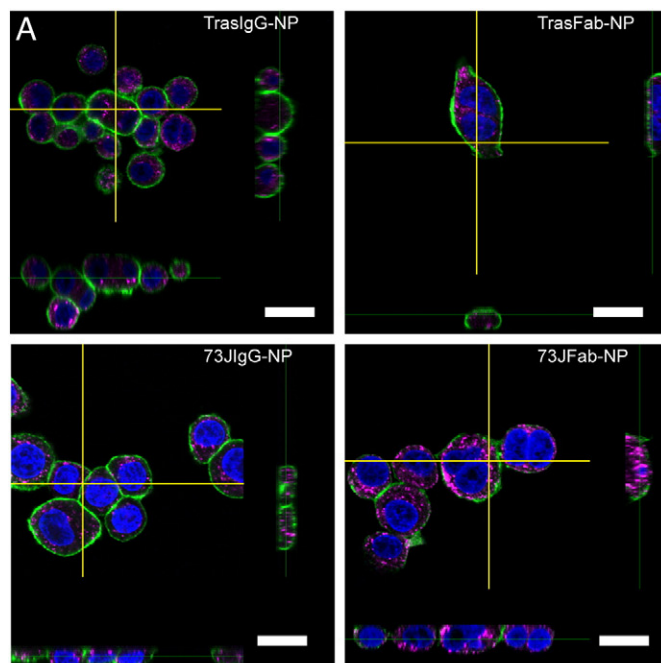


**Fig. 8.** Ab-NP conjugates traffic to lysosomes at significantly higher levels than the parent antibody. A) Confocal images of HER2 positive BT-474 cells show the location of anti-HER2 antibodies (green, anti-Human Fab), lysosomes (magenta, anti-LAMP2) and cell nuclei (blue, DAPI) (scale bar = 20  $\mu$ m). Distinct, punctate bodies seen in the images are indicative of lysosomal compartments. B, C) Conjugation with a polymeric nanoparticle (Ab-NP) significantly alters the amount of antibody that co-localizes with lysosomes in both B) BT-474 and C) SKBr-3 cell lines (mean  $\pm$  SD, N = 6, \*\*\*p < 0.001). Moreover, more of the 73JlgG-NP accumulates in the lysosome than TraslGg-NP in both BT-474 and SKBr-3 cells (mean  $\pm$  SD, N = 6, \*\*\*p < 0.001).

does not significantly alter lysosomal accumulation. Thus the efficacy associated with ADCC for full IgG forms is unlikely to be affected by small molecule conjugation; however, since most anti-cancer therapeutics act on intracellular targets and only 5–10% of the conjugated antibody was observed in the lysosome, this limited intracellular trafficking of the antibody–drug conjugates may constrain the efficacy of the conjugated drug. This underlines the importance of examining intracellular accumulation in other systems that are being pursued.

In this study, only two small molecules were coupled to each antibody. Increasing the number of small-molecules per antibody above ~5 SM/Ab has been shown to influence the pharmacokinetics of antibody–drug conjugates and may also influence the trafficking profile of Ab–SM [51] – at 2 SM/Ab in our system, this was not a concern. The SMCC conjugation that we used mirrors that used in the newly approved T-DM1; however, this chemical modification is non-specific. Emerging antibody–drug conjugates utilize site-specific modifications to control both the location and degree of substitution [52,53].

For Ab–NP conjugates, the cellular distribution is significantly different from Ab alone, resulting in 2–3 fold increase in the lysosomal accumulation of the Ab–NP compared to either the parent antibody or Ab–SM. Considering the increased intracellular accumulation over Ab and Ab–SM, and that Ab–NP can contain significantly greater drug per antibody, Ab–NPs should facilitate the delivery of significantly higher concentrations of chemotherapeutic agents inside the cell. Although increased payload delivery from nanoparticles is the central dogma of the field, few studies actually confirm cellular binding and lysosomal distribution of Ab–NP conjugates. Likely, both the size (100 nm) and the zeta potential (–21.1 mV) of the nanoparticle influence trafficking. These parameters are important in determining the mechanism of cell internalization and have been shown to induce non-clathrin forms of endocytosis in other Ab–NP systems [35–37].

By selecting antibodies that bind the same cell surface antigen but different epitopes, we demonstrate the importance of epitope binding to intracellular lysosomal accumulation, which will likely influence efficacy. Considering the impact that binding different epitopes of HER2 has on cell trafficking, 73JlgG presents a new antibody that itself may have therapeutic efficacy in addition to the targeting and lysosomal accumulation shown herein with both Ab–SM or Ab–NP systems [49]. The enhanced lysosomal accumulation of 73JlgG may be particularly useful for such applications that require payload delivery to the intracellular environment.

## 5. Conclusions

Anti-HER2 antibodies have already seen important clinical success and additional anti-HER2 antibodies can be designed from screening phage-displayed libraries. These synthetic antibodies bind to different epitopes than currently available antibodies and show a different distribution profile from trastuzumab. The binding kinetics, even at different pH, does not necessarily predict the cell trafficking profile of the antibodies, necessitating cell studies to elucidate the fate of therapeutic antibodies. Changes in cell trafficking become even more important for conjugates like trastuzumab–DM1 or antibody–nanoparticle conjugates that require delivery to subcellular compartments or organelles. Conjugating the antibodies to small molecules does not alter the cell trafficking profile; however, conjugating these antibodies to polymeric nanoparticles results in more antibodies trafficked to the lysosome. Altering the cell trafficking of antibody–conjugates may increase the amount of drug delivered to the cell but may also simultaneously influence the therapeutic mechanism of the parent antibody. As such, utilizing antibodies as targeting ligands for delivering large drug payloads should be thoroughly characterized for each system to prevent deleterious changes in cell distribution. Any modifications to an antibody may also alter the systemic pharmacokinetics of the conjugates and should likewise be monitored.

## Appendix A. Supplementary data

Supplementary data to this article can be found online at <http://dx.doi.org/10.1016/j.jconrel.2013.07.011>.

## References

- [1] N.E. Hynes, H.A. Lane, ERBB receptors and cancer: the complexity of targeted inhibitors, *Nat. Rev. Cancer* 5 (2005) 341–354.
- [2] J. Mendelsohn, J. Baselga, The EGF receptor family as targets for cancer therapy, *Oncogene* 19 (2000) 6550–6565.
- [3] K. Roepstorff, L. Grovdal, M. Grandal, M. Lerdrup, B. van Deurs, Endocytic downregulation of ErbB receptors: mechanisms and relevance in cancer, *Histochem. Cell Biol.* 129 (2008) 563–578.
- [4] C.A. Hudis, Trastuzumab – mechanism of action and use in clinical practice, *N. Engl. J. Med.* 357 (2007) 39–51.
- [5] J. Albanell, J. Codony, A. Rovira, B. Mellado, P. Gascon, Mechanism of action of anti-HER2 monoclonal antibodies: scientific update on trastuzumab and 2C4, in: A. Llombart-Bosch, V. Felipo (Eds.), *New Trends in Cancer for the 21st Century*, 2003, pp. 253–268.
- [6] J. Baselga, J. Albanell, Mechanism of action of anti-HER2 monoclonal antibodies, *Ann. Oncol.* 12 (2001) 35–41.
- [7] C.D. Austin, A.M. De Maziere, P.I. Pisacane, S.M. van Dijk, C. Eigenbrot, M.X. Sliwkowski, J. Klumperman, R.H. Scheller, Endocytosis and sorting of ErbB2 and the site of action of cancer therapeutics trastuzumab and geldanamycin, *Mol. Biol. Cell* 15 (2004) 5268–5282.
- [8] T. Vu, F.X. Claret, Trastuzumab: updated mechanisms of action and resistance in breast cancer, *Front. Oncol.* 2 (2012) 62–68.
- [9] M.V. Karamouzis, P.A. Konstantinopoulos, A.G. Papavassiliou, Trastuzumab – mechanism of action and use, *N. Engl. J. Med.* 357 (2007) 39–51.
- [10] M.X. Sliwkowski, J.A. Lofgren, G.D. Lewis, T.E. Hotaling, B.M. Fendly, J.A. Fox, Nonclinical studies addressing the mechanism of action of trastuzumab (Herceptin), *Semin. Oncol.* 26 (1999) 60–70.
- [11] A. Sorkin, L.K. Goh, Endocytosis and intracellular trafficking of ErbBs, *Exp. Cell Res.* 315 (2009) 683–696.
- [12] Y. Kitano, S. Umemura, H. Ohbayashi, M. Takenaga, R.Y. Osamura, Assessment of a new anti-HER2 monoclonal antibody, SV2-61 gamma: a best concordance with HER2 FISH, *Appl. Immunohistochem. Mol. Morphol.* 15 (2007) 389–393.
- [13] J.L. Nordstrom, S. Gorlatov, W. Zhang, Y. Yang, L. Huang, S. Burke, H. Li, V. Ciccarone, T. Zhang, J. Stavenhagen, S. Koenig, S.J. Stewart, P.A. Moore, S. Johnson, E. Bonvini, Anti-tumor activity and toxicokinetics analysis of MGAH22, an anti-HER2 monoclonal antibody with enhanced Fc gamma receptor binding properties, *Breast Cancer Res.* 13 (2011).
- [14] A.S. Tabatabaei-Panah, A.H. Zarnani, S. Montaser-Kouhsari, M. Chamankhah, R. Ghods, A.A. Bayat, G.E. Kazemi-Sefat, S.A.R. Mahmoudi, M.O. Karampour, S. Shojaeian, M. Jeddi-Tehrani, Production and characterizing anti-HER2 monoclonal antibodies, *Yakhteh* 10 (2008) 109–120.
- [15] A.L.A. Wong, S.-C. Lee, Mechanisms of resistance to trastuzumab and novel therapeutic strategies in HER2-positive breast cancer, *Int. J. Breast Cancer* 2012 (2012), (415170–415170).
- [16] J. Bostrom, L. Haber, P. Koenig, R.F. Kelley, G. Fuh, High affinity antigen recognition of the dual specific variants of Herceptin is entropy-driven in spite of structural plasticity, *PLoS One* 6 (2011) e17887.
- [17] S.S. Sidhu, S. Koide, Phage display for engineering and analyzing protein interaction interfaces, *Curr. Opin. Struct. Biol.* 17 (2007) 481–487.
- [18] F.A. Fellouse, K. Esaki, S. Birtalan, D. Raptis, V.J. Cancasci, A. Koide, P. Jhurani, M. Vasser, C. Wiesmann, A.A. Kossiakoff, S. Koide, S.S. Sidhu, High-throughput generation of synthetic antibodies from highly functional minimalist phage-displayed libraries, *J. Mol. Biol.* 373 (2007) 924–940.
- [19] H.K. Erickson, P.U. Park, W.C. Widdison, Y.V. Kovtun, L.M. Garrett, K. Hoffman, R.J. Lutz, V.S. Goldmacher, W.A. Blattler, Antibody-maytansinoid conjugates are activated in targeted cancer cells by lysosomal degradation and linker-dependent intracellular processing, *Cancer Res.* 66 (2006) 4426–4433.
- [20] S. Girish, M. Gupta, B. Wang, D. Lu, I.E. Krop, C.L. Vogel, H.A. Burris, P.M. LoRusso, J.H. Yi, O. Saad, B. Tong, Y.W. Chu, S. Holden, A. Joshi, Clinical pharmacology of trastuzumab emtansine (T-DM1): an antibody–drug conjugate in development for the treatment of HER2-positive cancer, *Cancer Chemother. Pharmacol.* 69 (2012) 1229–1240.
- [21] G.D. Lewis Phillips, G. Li, D.L. Dugger, L.M. Crocker, K.L. Parsons, E. Mai, W.A. Blattler, J.M. Lambert, R.V.J. Chari, R.J. Lutz, W.L.T. Wong, F.S. Jacobson, H. Koeppen, R.H. Schwall, S.R. Kenkare-Mitra, S.D. Spencer, M.X. Sliwkowski, Targeting HER2-positive breast cancer with trastuzumab–DM1, an antibody–cytotoxic drug conjugate, *Cancer Res.* 68 (2008) 9280–9290.
- [22] M. Shi, K. Ho, A. Keating, M.S. Shoichet, Doxorubicin-conjugated immunonanoparticles for intracellular anticancer drug delivery, *Adv. Funct. Mater.* 19 (2009) 1689–1696.
- [23] V.P. Torchilin, Targeted polymeric micelles for delivery of poorly soluble drugs, *Cell. Mol. Life Sci.* 61 (2004) 2549–2559.
- [24] E. Wagner, Programmed drug delivery: nanosystems for tumor targeting, *Expert. Opin. Biol. Ther.* 7 (2007) 587–593.
- [25] Y. Cheng, L. Zhao, Y. Li, T. Xu, Design of biocompatible dendrimers for cancer diagnosis and therapy: current status and future perspectives, *Chem. Soc. Rev.* 40 (2011) 2673–2703.

- [26] Y. Namiki, T. Fuchigami, N. Tada, R. Kawamura, S. Matsunuma, Y. Kitamoto, M. Nakagawa, Nanomedicine for cancer: lipid-based nanostructures for drug delivery and monitoring, *Acc. Chem. Res.* 44 (2011) 1080–1093.
- [27] L. Nobs, F. Buchegger, R. Gurny, E. Allemann, Current methods for attaching targeting ligands to liposomes and nanoparticles, *J. Pharm. Sci.* 93 (2004) 1980–1992.
- [28] C.J. Sunderland, M. Steiert, J.E. Talmadge, A.M. Derfus, S.E. Barry, Targeted nanoparticles for detecting and treating cancer, *Drug Dev. Res.* 67 (2006) 70–93.
- [29] E.L. Sievers, P.D. Senter, Antibody–drug conjugates in cancer therapy, *Annu. Rev. Med.* 64 (2013) 15–29.
- [30] F. Fay, C.J. Scott, Antibody-targeted nanoparticles for cancer therapy, *Immunotherapy* 3 (2011) 381–394.
- [31] D. Schrama, R.A. Reisfeld, J.C. Becker, Antibody targeted drugs as cancer therapeutics, *Nat. Rev. Drug Discov.* 5 (2006) 147–159.
- [32] T. Junttila, G. Li, K. Parsons, G. Phillips, M. Sliwkowski, Trastuzumab-DM1 (T-DM1) retains all the mechanisms of action of trastuzumab and efficiently inhibits growth of lapatinib insensitive breast cancer, *Breast Cancer Res. Treat.* 128 (2011) 347–356.
- [33] M.S.K. Sutherland, R.J. Sanderson, K.A. Gordon, J. Andreyka, C.G. Cerveney, C.P. Yu, T.S. Lewis, D.L. Meyer, R.F. Zabinski, S.O. Doronina, P.D. Senter, C.L. Law, A.F. Wahl, Lysosomal trafficking and cysteine protease metabolism confer target-specific cytotoxicity by peptide-linked anti-CD30-auristatin conjugates, *J. Biol. Chem.* 281 (2006) 10540–10547.
- [34] P.D. Senter, E.L. Sievers, The discovery and development of brentuximab vedotin for use in relapsed Hodgkin lymphoma and systemic anaplastic large cell lymphoma, *Nature Biotech* 30 (2012) 631–637.
- [35] S. Bhattacharyya, R.D. Singh, R. Pagano, J.D. Robertson, R. Bhattacharya, P. Mukherjee, Switching the targeting pathways of a therapeutic antibody by nanodesign, *Angew. Chem. Int. Ed.* 51 (2012) 1563–1567.
- [36] S. Bhattacharyya, R. Bhattacharya, S. Curley, M.A. McNiven, P. Mukherjee, Nanoconjugation modulates the trafficking and mechanism of antibody induced receptor endocytosis, *Proc. Natl. Acad. Sci. U. S. A.* 107 (2010) 14541–14546.
- [37] J. Liu, P. Kopeckova, P. Buehler, P. Wolf, H. Pan, H. Bauer, U. Elsaesser-Beile, J. Kopecek, Biorecognition and subcellular trafficking of HPMA copolymer-anti-PSMA antibody conjugates by prostate cancer cells, *Mol. Pharm.* 6 (2009) 959–970.
- [38] M. Shi, J.H. Wosnick, K. Ho, A. Keating, M.S. Shoichet, Immuno-polymeric nanoparticles by Diels–Alder chemistry, *Angew. Chem. Int. Ed. Engl.* 46 (2007) 6126–6131.
- [39] J. Lu, M.S. Shoichet, Self-assembled polymeric nanoparticles of organocatalytic copolymerized D, L-lactide and 2-methyl 2-carboxytrimethylene carbonate, *Macromolecules* 43 (2010) 4943–4953.
- [40] G.C. Howard, M.R. Kaser, Making and Using Antibodies: A Practical Handbook, Taylor & Francis, 2006.
- [41] J. Lu, S.C. Owen, M.S. Shoichet, Stability of self-assembled polymeric micelles in serum, *Macromolecules* 44 (2011) 6002–6008.
- [42] D.P.Y. Chan, S.C. Owen, M.S. Shoichet, Double click: dual functionalized polymeric micelles with antibodies and peptides, *Bioconjug. Chem.* 24 (2013) 105–113.
- [43] G.C. Howard, M.R. Kaser, Making and Using Antibodies: A Practical Handbook, CRC/Taylor & Francis, Boca Raton, FL, 2007.
- [44] K.W. Dunn, M.M. Kamocka, J.H. McDonald, A practical guide to evaluating colocalization in biological microscopy, *Am. J. Physiol. Cell Physiol.* 300 (2011) C723–C742.
- [45] J. Kao, K. Salari, M. Bocanegra, Y.L. Choi, L. Girard, J. Gandhi, K.A. Kwei, T. Hernandez-Boussard, P. Wang, A.F. Gazdar, J.D. Minna, J.R. Pollack, Molecular profiling of breast cancer cell lines defines relevant tumor models and provides a resource for cancer gene discovery, *PLoS One* 4 (2009).
- [46] J.R. Casey, S. Grinstein, J. Orłowski, Sensors and regulators of intracellular pH, *Nat. Rev. Mol. Cell Biol.* 11 (2010) 50–61.
- [47] L. Neckers, Hsp90 inhibitors as novel cancer chemotherapeutic agents, *Trends Mol. Med.* 8 (2002) S55–S61.
- [48] W.C. Widdison, S.D. Wilhelm, E.E. Cavanagh, K.R. Whiteman, B.A. Leece, Y. Kovtun, V.S. Goldmacher, H.S. Xie, R.M. Steeves, R.J. Lutz, R. Zhao, L.T. Wang, W.A. Blattler, R.V.J. Chari, Semisynthetic maytansine analogues for the targeted treatment of cancer, *J. Med. Chem.* 49 (2006) 4392–4408.
- [49] G. Valabrega, F. Montemurro, M. Aglietta, Trastuzumab: mechanism of action, resistance and future perspectives in HER2-overexpressing breast cancer, *Ann. Oncol.* 18 (2007) 977–984.
- [50] P. Nagy, E. Friedlander, M. Tanner, A.I. Kapanen, K.L. Carraway, J. Isola, T.M. Jovin, Decreased accessibility and lack of activation of ErbB2 in JIMT-1, a Herceptin-resistant, MUC4-expressing breast cancer cell line, *Cancer Res.* 65 (2005) 473–482.
- [51] K. Lin, J. Tibbitts, Pharmacokinetic considerations for antibody drug conjugates, *Pharm. Res.* 29 (2012) 2354–2366.
- [52] J.Y. Axup, K.M. Bajjuri, M. Ritland, B.M. Hutchins, C.H. Kim, S.A. Kazane, R. Halder, J.S. Forsyth, A.F. Santidrian, K. Stafin, Y. Lu, T. Hon, A.J. Seller, S.L. Biroce, A. Szydluk, J.K. Pinkstaff, F. Tian, S.C. Sinha, B. Felding-Habermann, V.V. Smider, P.G. Schultz, Synthesis of site-specific antibody–drug conjugates using unnatural amino acids, *Proc. Natl. Acad. Sci. U. S. A.* 109 (2012) 16101–16106.
- [53] A.M. Wu, P.D. Senter, Arming antibodies: prospects and challenges for immunoconjugates, *Nat. Biotechnol.* 23 (2005) 1137–1146.